Composite Structures 178 (2017) 37–49

Contents lists available at ScienceDirect

Composite Structures

journal homepage: www.elsevier.com/locate/compstruct

An efficient warping model for elastoplastic torsional analysis of composite beams

Kyungho Yoon [a], Phill-Seung Lee [b], Do-Nyun Kim [a,c,*]

[a] Department of Mechanical and Aerospace Engineering, Seoul National University, Gwanak-ro 1, Gwanak-gu, Seoul 08826, Republic of Korea
[b] Department of Mechanical Engineering, Korea Advanced Institute of Science and Technology, 291 Daehak-ro, Yuseong-gu, Daejeon 34141, Republic of Korea
[c] Institute of Advanced Machines and Design, Seoul National University, Gwanak-ro 1, Gwanak-gu, Seoul 08826, Republic of Korea

ARTICLE INFO

Article history:
Received 14 February 2017
Revised 18 May 2017
Accepted 13 July 2017
Available online 18 July 2017

Keywords:
Composite beam
Torsion
Warping
Elastoplasticity
Finite element method

ABSTRACT

In this paper, we present an efficient warping model for nonlinear elastoplastic torsional analysis of composite beams developed based on Benscoter warping theory. A major challenge here is how to account for the evolution of warping functions efficiently as materials yield at various locations at different rates. Here, we propose to describe the warping displacement using a linear combination of two asymptotic warping functions with corresponding warping degrees of freedom. The asymptotic warping functions are calculated only once initially by solving the extended St. Venant equations under two material conditions: purely elastic condition and fully plastic condition when no material point in the cross-section remains elastic. Only the warping degrees of freedom are updated incrementally and iteratively in analysis without evaluating the warping functions again. The proposed warping model demonstrates an excellent performance in several numerical examples despite its simplicity.

1. Introduction

Composite beams have been widely used in many engineering fields due to their excellent mechanical properties such as high specific stiffness and strength and improved fracture toughness as well as the design flexibility to meet the target properties [1–3]. It is essential for proper applications to understand their nonlinear mechanical behaviors under various structural loads considering the complexity in geometry and material composition. Numerous numerical methods have been developed for analysis of composite beams with a particular focus on the formulation of efficient beam models [4–16], where incorporating the warping effect efficiently into the beam formulation is crucial as it affects significantly the nonlinear behavior of composite beams particularly with arbitrary cross-sections. Although considerable research has been devoted to develop the warping model for composite beams under torsion [17–24], investigations have been confined to elastic deformation and little attention has been paid to elastoplastic warping models.

The most challenging part in formulating a torsion theory including warping under elastoplastic condition is how to reflect the change of warping functions effectively as plastic deformations accumulate at various rates and locations. Sapountzakis and Tsipiras [25] looked into this problem for the first time and proposed a warping function considering the progress of yield regions applied to the boundary element method. However, their formulation is limited to prismatic beams under pure torsional moments only. Furthermore, the warping function should be evaluated newly in every incremental step, which is computationally expensive.

In this paper, we present an efficient approach to considering the warping effect in nonlinear elastoplastic torsional analysis of 3D composite beams using the finite element method. The proposed method employs the essential philosophy of Benscoter-type warping consideration [26–28] and the extended warping theory used for elastic deformation [19,21,24]. It describes the warping displacement using two asymptotic warping functions obtained by solving the extended St. Venant equations assuming a purely elastic condition where no plastic deformation occurs and a fully plastic condition where every material point in the cross-section experiences the plastic deformation. These warping functions are calculated only once initially and used without reevaluation during the solution procedure. Only the corresponding warping degrees of freedom (DOFs) are updated incrementally and iteratively. Moreover, the formulation is dependent neither on the warping boundary condition (free or constrained) nor on the topology of cross-sections (simply- or multiply-connected).

* Corresponding author at: Department of Mechanical and Aerospace Engineering, Seoul National University, Gwanak-ro 1, Gwanak-gu, Seoul 08826, Republic of Korea.
E-mail address: dnkim@snu.ac.kr (D.-N. Kim).

http://dx.doi.org/10.1016/j.compstruct.2017.07.041
0263-8223/

This warping model is incorporated into our continuum mechanics based beam element [16–17,28,31] so that important nonlinear effects such as Wagner strain and von Kármán strain can be naturally considered. Since the formulation is based on continuum mechanics, it is capable of handling complicate 3D composite beams with arbitrary cross-sectional shapes in geometric and/or materially nonlinear analysis.

This paper is organized as follows. We present the kinematic description of the proposed beam element including the warping displacements in Section 2 and how to evaluate the asymptotic warping functions in Section 3. In Section 4, we provide the beam finite element formulation for nonlinear analysis followed by several numerical examples in Section 5 to demonstrate the efficiency and accuracy of the proposed method. Finally, we conclude with summary and future directions in Section 6.

2. Kinematic description

We begin with describing the kinematics of the continuum mechanics based beam element [16,28,31] that is directly degenerated from a solid finite element model consisting of partitioned sub-beams (Fig. 1). The position vector of a material point in sub-beam m at time t, ${}^t\mathbf{x}^{(m)}$, is given as

$$ {}^t\mathbf{x}^{(m)} = \sum_{k=1}^{q} h_k(\varsigma)\,{}^t\mathbf{x}_k + \sum_{k=1}^{q} h_k(\varsigma) \sum_{j=1}^{\bar{q}} h_j(\xi,\eta)\,\bar{y}_k^{j(m)}\,{}^t\mathbf{V}_{\bar{y}}^k + \sum_{k=1}^{q} h_k(\varsigma) \sum_{j=1}^{\bar{q}} h_j(\xi,\eta)\,\bar{z}_k^{j(m)}\,{}^t\mathbf{V}_{\bar{z}}^k \quad (1) $$

where $h_k(\varsigma)$ is the 1D shape function along the longitudinal axis, ${}^t\mathbf{x}_k$ is the position vector of beam node k, ${}^t\mathbf{V}_{\bar{y}}^k$ and ${}^t\mathbf{V}_{\bar{z}}^k$ are the orthonormal director vectors of the cross-section at beam node k, $\bar{y}_k^{j(m)}$ and $\bar{z}_k^{j(m)}$ are the coordinates of cross-sectional node j in sub-beam m with the corresponding 2D shape function $h_j(\xi,\eta)$, q is the total number of nodes of a beam element while $\bar{q}$ is the total number of nodes of a cross-sectional element, and ς, ξ, and η in parenthesis are natural coordinates. This kinematic description can represent Timoshenko's six deformation modes of a beam: one stretching mode, two transverse shearing modes, one twisting mode, and two bending modes.

In order to consider the warping effect, we use an enriched kinematic description based on Benscoter warping theory that can be written for sub-beam m as

$$ {}^t\mathbf{x}_e^{(m)} = {}^t\mathbf{x}^{(m)} + {}^t\mathbf{x}_w^{(m)} \text{ with } {}^t\mathbf{x}_w^{(m)} = \sum_{k=1}^{q} h_k(\varsigma) \sum_{j=1}^{\bar{q}} h_j(\xi,\eta) f^{j(m)}\,{}^t\alpha_k\,{}^t\mathbf{V}_{\bar{x}}^k \quad (2) $$

where $f^{j(m)}$ is the value of the warping function at cross-sectional node j obtained by solving the extended St. Venant equations [19,21,24], ${}^t\alpha_k$ is the warping DOF at beam node k, and ${}^t\mathbf{V}_{\bar{x}}^k$ is the warping director vector orthonormal to ${}^t\mathbf{V}_{\bar{y}}^k$ and ${}^t\mathbf{V}_{\bar{z}}^k$. This enriched description can represent the continuous and compatible 3D kinematics of the warping deformation through interpolation of the warping function along the longitudinal direction using the nodal warping DOF and director vector. It is noteworthy that here the warping function is assumed to remain unchanged as in Benscoter warping theory. In other words, only the magnitude and the direction of the warping displacements change during deformation while their spatial distribution on a cross-section is preserved. This rather simple enrichment for the warping deformation has proven to be successful to describe the nonlinear torsional behavior of composite beams in elastic regime [16,17,19,20,26].

The above kinematic description is, however, not able to describe the warping behavior of composite beams properly when materials begin to yield. It is because the plastic deformation may occur at different locations at different rates leading to inhomogeneous and time-varying distribution of material properties on the cross-section. As a result, the warping function itself evolves with the plastic deformation since the extended St. Venant equations determining the warping function are dependent on the spatial variation of moduli for composite materials. Therefore, we need to update, in principle, the warping function continuously by solving the extended St. Venant equations, which is computationally inefficient.

To circumvent this problem, we propose a simple extension of the above kinematic description for elastoplastic analysis by approximating the warping displacement on a cross-section as a linear combination of two asymptotic warping functions. The position vector using the newly proposed warping model can be written as

$$ {}^t\mathbf{x}_e^{(m)} = {}^t\mathbf{x}^{(m)} + {}^t\mathbf{x}_w^{(m)} \text{ with } {}^t\mathbf{x}_w^{(m)} = \sum_{k=1}^{q} h_k(\varsigma) \sum_{j=1}^{\bar{q}} [h_j(\xi,\eta) f_e^{j(m)}\,{}^t\alpha_k^e + h_j(\xi,\eta) f_p^{j(m)}\,{}^t\alpha_k^p]\,{}^t\mathbf{V}_{\bar{x}}^k, \quad (3) $$

where $f_e^{j(m)}$ and $f_p^{j(m)}$ are the values of the asymptotic elastic and plastic warping functions, respectively, at cross-sectional node j, and ${}^t\alpha_k^e$ and ${}^t\alpha_k^p$ are the corresponding warping DOFs at beam node

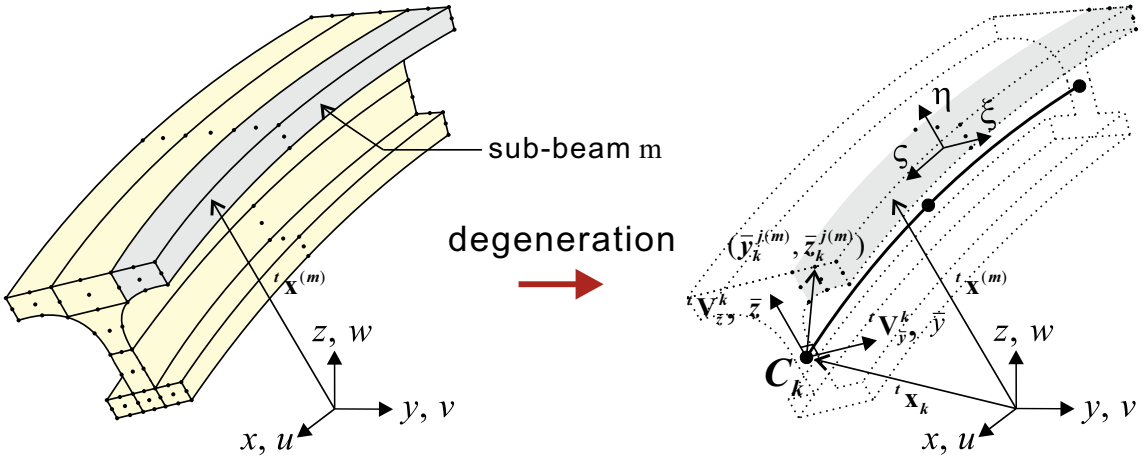

Fig. 1. The direct degeneration concept of the continuum mechanics based beam finite element.

k. The asymptotic warping functions are calculated only once initially and remain unchanged during nonlinear analysis so that the warping DOFs and director vectors are only updated incrementally and iteratively. The elastic warping function is calculated by solving the extended St. Venant equations using the elastic moduli while the elastoplastic tangent moduli are used instead for the calculation of the asymptotic plastic warping function assuming that all material points deform plastically as described in detail in the following section.

3. Calculation of the asymptotic warping functions

In this section, we present our finite element procedure to calculate two asymptotic warping functions required to construct the warping displacement in Eq. (3) before performing nonlinear analysis. Two Cartesian coordinate systems are defined on the cross-section at beam node k: $(\bar{y},\bar{z})$ with its origin at the beam node position C_k and $(\hat{y},\hat{z})$ with its origin at the twist center $\hat{C}_k$ denoted as $(\lambda_{\bar{y}}, \lambda_{\bar{z}})$ (Figs. 1 and 2). The composite cross-section is discretized by sub-domains $\Omega^{(m)}$, each of which is modeled as an elastoplastic material as shown in Fig. 3.

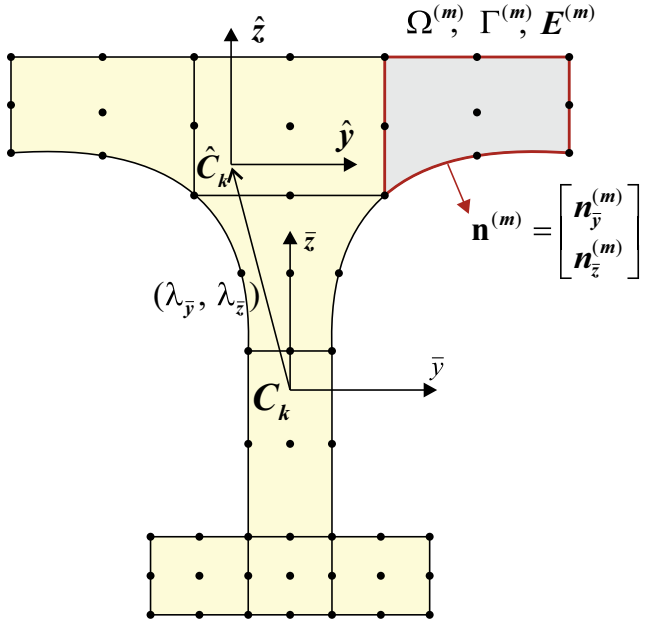

Fig. 2. A discretized cross-section at beam node k.

3.1. Elastic warping function

To calculate the asymptotic elastic warping function $f_e^{j(m)}$ in Eq. (3), we assume that the entire cross-sectional domains are under purely elastic condition and sub-domain $\Omega^{(m)}$ has the elastic and shear moduli, $E_e^{(m)}$ and $G_e^{(m)}$, respectively. Then, the discretized form of the extended St. Venant equations [19,21,24] on a beam cross-section can be written for each sub-domain as

$$G_e^{(m)}\left(\frac{\partial^2 f_e^{(m)}}{\partial \hat{y}^2}+\frac{\partial^2 f_e^{(m)}}{\partial \hat{z}^2}\right)=0 \quad \text{in} \quad \Omega^{(m)} \tag{4a}$$

$$G_e^{(m)}\frac{\partial f_e^{(m)}}{\partial \mathbf{n}^{(m)}}=G_e^{(m)}\left(n_{\bar{y}}^{(m)}\hat{z}^{(m)}-n_{\bar{z}}^{(m)}\hat{y}^{(m)}\right) \quad \text{on} \quad \Gamma^{(m)} \tag{4b}$$

where $f_e^{(m)}$ is the elastic warping function and $\mathbf{n}^{(m)}=[\,n_{\bar{y}}^{(m)} \quad n_{\bar{z}}^{(m)}\,]^T$ is a unit vector normal to the boundary $\Gamma^{(m)}$. The weak form of Eq. (4a) can be obtained by introducing a virtual elastic warping function $\delta f_e^{(m)}$ and summing the equations over sub-domains as

$$\sum_{m=1}^{n}\left[\int_{\Omega^{(m)}} G_e^{(m)}\left(\frac{\partial f_e^{(m)}}{\partial \hat{y}}\frac{\partial \delta f_e^{(m)}}{\partial \hat{y}}+\frac{\partial f_e^{(m)}}{\partial \hat{z}}\frac{\partial \delta f_e^{(m)}}{\partial \hat{z}}\right)d\Omega^{(m)}\right] = \sum_{m=1}^{n}\left[\int_{\Gamma^{(m)}} G_e^{(m)}\frac{\partial f_e^{(m)}}{\partial \mathbf{n}^{(m)}}\delta f_e^{(m)}d\Gamma^{(m)}\right]. \tag{5}$$

Incorporating Eq. (4b) into Eq. (5), the variational form of the extended St. Venant equation can be derived as

$$\sum_{m=1}^{n}\left[\int_{\Omega^{(m)}} G_e^{(m)}\left(\frac{\partial f_e^{(m)}}{\partial \hat{y}}\frac{\partial \delta f_e^{(m)}}{\partial \hat{y}}+\frac{\partial f_e^{(m)}}{\partial \hat{z}}\frac{\partial \delta f_e^{(m)}}{\partial \hat{z}}\right)d\Omega^{(m)}\right] = \sum_{m=1}^{n}\left[\int_{\Gamma^{(m)}} G_e^{(m)}(n_{\bar{y}}^{(m)}\hat{z}^{(m)}-n_{\bar{z}}^{(m)}\hat{y}^{(m)})\delta f_e^{(m)}d\Gamma^{(m)}\right]. \tag{6}$$

Since $\hat{y}=\bar{y}-\lambda_{\bar{y}}$ and $\hat{z}=\bar{z}-\lambda_{\bar{z}}$, Eq. (6) becomes

$$\begin{aligned}&\sum_{m=1}^{n}\left[\int_{\Omega^{(m)}} G_e^{(m)}\left(\frac{\partial f_e^{(m)}}{\partial \bar{y}}\frac{\partial \delta f_e^{(m)}}{\partial \bar{y}}+\frac{\partial f_e^{(m)}}{\partial \bar{z}}\frac{\partial \delta f_e^{(m)}}{\partial \bar{z}}\right)d\Omega^{(m)}\right]\\ &+\sum_{m=1}^{n}\left[\int_{\Gamma^{(m)}} G_e^{(m)}\lambda_{\bar{z}}n_{\bar{y}}^{(m)}\delta f_e^{(m)}d\Gamma^{(m)}\right]\\ &-\sum_{m=1}^{n}\left[\int_{\Gamma^{(m)}} G_e^{(m)}\lambda_{\bar{y}}n_{\bar{z}}^{(m)}\delta f_e^{(m)}d\Gamma^{(m)}\right]\\ &=\sum_{m=1}^{n}\left[\int_{\Gamma^{(m)}} G_e^{(m)}(n_{\bar{y}}^{(m)}\bar{z}^{(m)}-n_{\bar{z}}^{(m)}\bar{y}^{(m)})\delta f_e^{(m)}d\Gamma^{(m)}\right].\end{aligned} \tag{7}$$

Applying the zero bending moment conditions ($M_{\bar{z}}=M_{\bar{y}}=0$) for beams under pure torsion gives

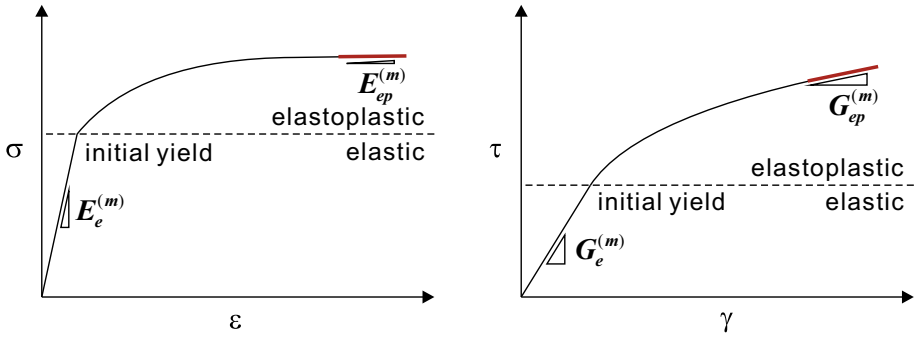

Fig. 3. An elastoplastic material law. Red lines represent the asymptotic elastoplastic tangent moduli. (For interpretation of the references to colour in this figure legend, the reader is referred to the web version of this article.)

$$\sum_{m=1}^{n}\left[\int_{\Omega^{(m)}} E_e^{(m)} f_e^{(m)}(\bar{y}-\bar{y}_{ave})d\Omega^{(m)}\right]=0, \tag{8a}$$

$$\sum_{m=1}^{n}\left[\int_{\Omega^{(m)}} E_e^{(m)} f_e^{(m)}(\bar{z}-\bar{z}_{ave})d\Omega^{(m)}\right]=0, \tag{8b}$$

where $(\bar{y}_{ave}, \bar{z}_{ave})$ represents the centroid of the cross-section written as

$$\bar{y}_{ave}=\frac{\sum_{m=1}^{n}\int_{\Omega^{(m)}}\bar{y}d\Omega^{(m)}}{\sum_{m=1}^{n}\int_{\Omega^{(m)}}d\Omega^{(m)}} \quad \text{and} \quad \bar{z}_{ave}=\frac{\sum_{m=1}^{n}\int_{\Omega^{(m)}}\bar{z}d\Omega^{(m)}}{\sum_{m=1}^{n}\int_{\Omega^{(m)}}d\Omega^{(m)}} \tag{9}$$

In sub-domain $\Omega^{(m)}$, we interpolate the warping function as

$$f_e^{(m)}=\mathbf{H}^{(m)}\mathbf{F}_e^{(m)}=\mathbf{H}^{(m)}\mathbf{L}^{(m)}\mathbf{F}_e, \tag{10}$$

where

$$\mathbf{H}^{(m)}=\begin{bmatrix}h_1(\xi,\eta) & h_2(\xi,\eta) & \cdots & h_{\bar{q}}(\xi,\eta)\end{bmatrix}, \tag{11a}$$

$$\mathbf{F}_e^{(m)}=\begin{bmatrix}f_e^{1(m)} & f_e^{2(m)} & \cdots & f_e^{\bar{q}(m)}\end{bmatrix}^T, \tag{11b}$$

$$\mathbf{F}_e=\begin{bmatrix}f_e^{1} & f_e^{2} & \cdots & f_e^{l}\end{bmatrix}^T. \tag{11c}$$

Here, $\mathbf{L}^{(m)}$ is the standard assemblage Boolean matrix for cross-sectional element m that relates $\mathbf{F}_e^{(m)}$, a vector containing the values of the elastic warping function at the nodes in $\Omega^{(m)}$, to $\mathbf{F}_e$, a vector with the values of the elastic warping function at the nodes in the entire cross-section. $h_j(\xi,\eta)$ is the 2D shape function corresponding to cross-sectional node j and l denotes the total number of cross-sectional nodes.

Then, we can obtain the final set of equations in matrix form used to calculate the nodal values of the elastic warping function and the coordinates of the twist center simultaneously as

$$\begin{bmatrix}\mathbf{K} & \mathbf{N}_{\bar{y}} & \mathbf{N}_{\bar{z}}\\ \mathbf{H}_{\bar{y}} & \mathbf{0} & \mathbf{0}\\ \mathbf{H}_{\bar{z}} & \mathbf{0} & \mathbf{0}\end{bmatrix}\begin{bmatrix}\mathbf{F}_e\\ \lambda_{\bar{z}}\\ \lambda_{\bar{y}}\end{bmatrix}=\begin{bmatrix}\mathbf{B}\\ 0\\ 0\end{bmatrix}, \tag{12}$$

where

$$\mathbf{K}=\sum_{m=1}^{n}\left[\int_{\Omega^{(m)}} G_e^{(m)}\mathbf{L}^{(m)^T}\left(\frac{\partial\mathbf{H}^{(m)^T}}{\partial\bar{y}}\frac{\partial\mathbf{H}^{(m)}}{\partial\bar{y}}+\frac{\partial\mathbf{H}^{(m)^T}}{\partial\bar{z}}\frac{\partial\mathbf{H}^{(m)}}{\partial\bar{z}}\right)\mathbf{L}^{(m)}d\Omega^{(m)}\right], \tag{13a}$$

$$\mathbf{N}_{\bar{y}}=\sum_{m=1}^{n}\left[\int_{\Omega^{(m)}} G_e^{(m)}n_{\bar{y}}^{(m)}\mathbf{L}^{(m)^T}\mathbf{H}^{(m)^T}d\Omega^{(m)}\right], \tag{13b}$$

$$\mathbf{N}_{\bar{z}}=\sum_{m=1}^{n}\left[\int_{\Omega^{(m)}} G_e^{(m)}n_{\bar{z}}^{(m)}\mathbf{L}^{(m)^T}\mathbf{H}^{(m)^T}d\Omega^{(m)}\right], \tag{13c}$$

$$\mathbf{B}=\sum_{m=1}^{n}\left[\int_{\Gamma^{(m)}} G_e^{(m)}(n_{\bar{y}}^{(m)}\bar{z}^{(m)}-n_{\bar{z}}^{(m)}\bar{y}^{(m)})\mathbf{L}^{(m)^T}\mathbf{H}^{(m)^T}d\Gamma^{(m)}\right], \tag{13d}$$

$$\mathbf{H}_{\bar{y}}=\sum_{m=1}^{n}\left[\int_{\Omega^{(m)}} E_e^{(m)}(\bar{y}-\bar{y}_{ave})\mathbf{H}^{(m)}\mathbf{L}^{(m)}d\Omega^{(m)}\right], \tag{13e}$$

$$\mathbf{H}_{\bar{z}}=\sum_{m=1}^{n}\left[\int_{\Omega^{(m)}} E_e^{(m)}(\bar{z}-\bar{z}_{ave})\mathbf{H}^{(m)}\mathbf{L}^{(m)}d\Omega^{(m)}\right]. \tag{13f}$$

3.2. Plastic warping function

The procedure to calculate the asymptotic plastic warping function $f_p^{i(m)}$ in Eq. (3) is the same as the one for the elastic warping function except that elastoplastic tangent moduli must be used instead of elastic ones in Eq. (13) assuming that sufficiently large plastic deformations are developed in the entire cross-sectional domains. The asymptotic elastoplastic tangent moduli $E_{ep}^{(m)}$ and $G_{ep}^{(m)}$, for sub-domain $\Omega^{(m)}$ can be defined analytically using the condition where either uniaxial tension or pure shear is applied to the material, respectively (Fig. 3). To illustrate, theses moduli for materials that can be modeled using the von Mises yield criterion with the associated flow rule and the isotropic hardening can be obtained as follows.

The von Mises yield function $\Phi^{(m)}$ with an isotropic hardening model can be written as

$$\Phi^{(m)}(\tilde{\sigma}^{(m)},\sigma_y^{(m)})=\tilde{\sigma}^{(m)}-\sigma_y^{(m)}=0 \tag{14a}$$

$$\text{with } \tilde{\sigma}^{(m)}=\sqrt{\frac{3}{2}\sigma_{ij}^{(m)}\sigma_{ij}^{(m)}-\frac{1}{2}(\sigma_{ij}^{(m)})^2} \tag{14b}$$

where $\tilde{\sigma}^{(m)}$ denotes the effective stress and $\sigma_y^{(m)}$ is the yield stress which is given as a function of an internal hardening variable such as the equivalent plastic strain $\tilde{\varepsilon}_p^{(m)}$ defined as

$$\tilde{\varepsilon}_p^{(m)}=\int\sqrt{\frac{2}{3}\dot{\varepsilon}_{p,ij}^{(m)}\dot{\varepsilon}_{p,ij}^{(m)}}\,dt, \tag{15}$$

in which $\dot{\varepsilon}_{p,ij}^{(m)}$ is the plastic strain rate.

Then, $E_{ep}^{(m)}$ can be obtained by assuming an uniaxial tension case where the uniaxial stress $\sigma^{(m)}$ and strain $\varepsilon^{(m)}$ are only considered such that the von Mises effective stress and strain are simplified as $\tilde{\sigma}^{(m)}=\sigma^{(m)}$ and $\tilde{\varepsilon}^{(m)}=\varepsilon^{(m)}$, respectively. The elastoplastic tangent modulus becomes

$$E_{ep}^{(m)}=\frac{\partial\sigma^{(m)}}{\partial\varepsilon^{(m)}}. \tag{16}$$

Under plastic flow condition, the value of the yield function remains zero leading to $\sigma^{(m)}=\sigma_y^{(m)}$. Hence, if we define the hardening modulus which would be a function of the equivalent plastic strain as

$$H^{(m)}=\frac{\partial\sigma_y^{(m)}}{\partial\varepsilon_p^{(m)}}=\frac{\partial\sigma^{(m)}}{\partial\varepsilon_p^{(m)}} \tag{17}$$

and use $E_e^{(m)}=\partial\sigma^{(m)}/\partial\varepsilon_e^{(m)}$, then Eq. (16) can be written as

$$E_{ep}^{(m)}=\frac{H^{(m)}E_e^{(m)}}{H^{(m)}+E_e^{(m)}}. \tag{18}$$

Similarly, $G_{ep}^{(m)}$ can be obtained by assuming a pure shear case where the shear stress $\tau^{(m)}$ and strain $\gamma^{(m)}$ on a plane are only considered resulting in $\tilde{\sigma}^{(m)}=\sqrt{3}\tau^{(m)}$ and $\tilde{\varepsilon}^{(m)}=\gamma^{(m)}/\sqrt{3}$. The elastoplastic shear tangent modulus becomes

$$G_{ep}^{(m)}=\frac{\partial\tau^{(m)}}{\partial\gamma^{(m)}}. \tag{19}$$

Since the hardening modulus is the same as in the previous uniaxial tension case

$$\frac{\partial\tau^{(m)}}{\partial\gamma_p^{(m)}}=\frac{\partial\tilde{\sigma}^{(m)}/\sqrt{3}}{\sqrt{3}\partial\tilde{\varepsilon}^{(m)}}=\frac{1}{3}H^{(m)} \tag{20}$$

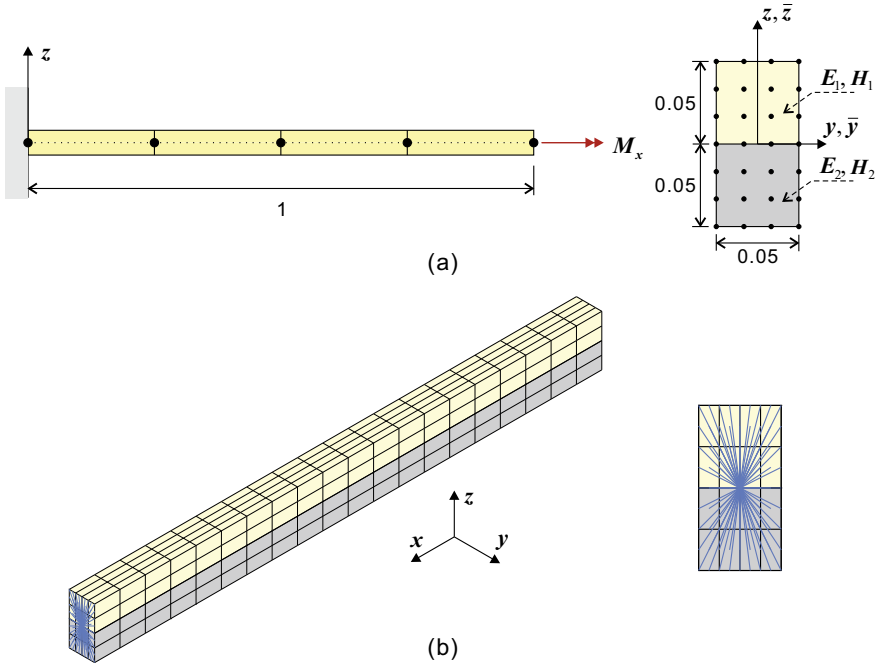

Fig. 4. Double layered beam problem (unit: *m*): (a) beam model (four beam elements along the beam axis, two cubic cross-sectional elements, 40 DOFs in total) and (b) solid model (320 solid elements, 9963 DOFs in total).

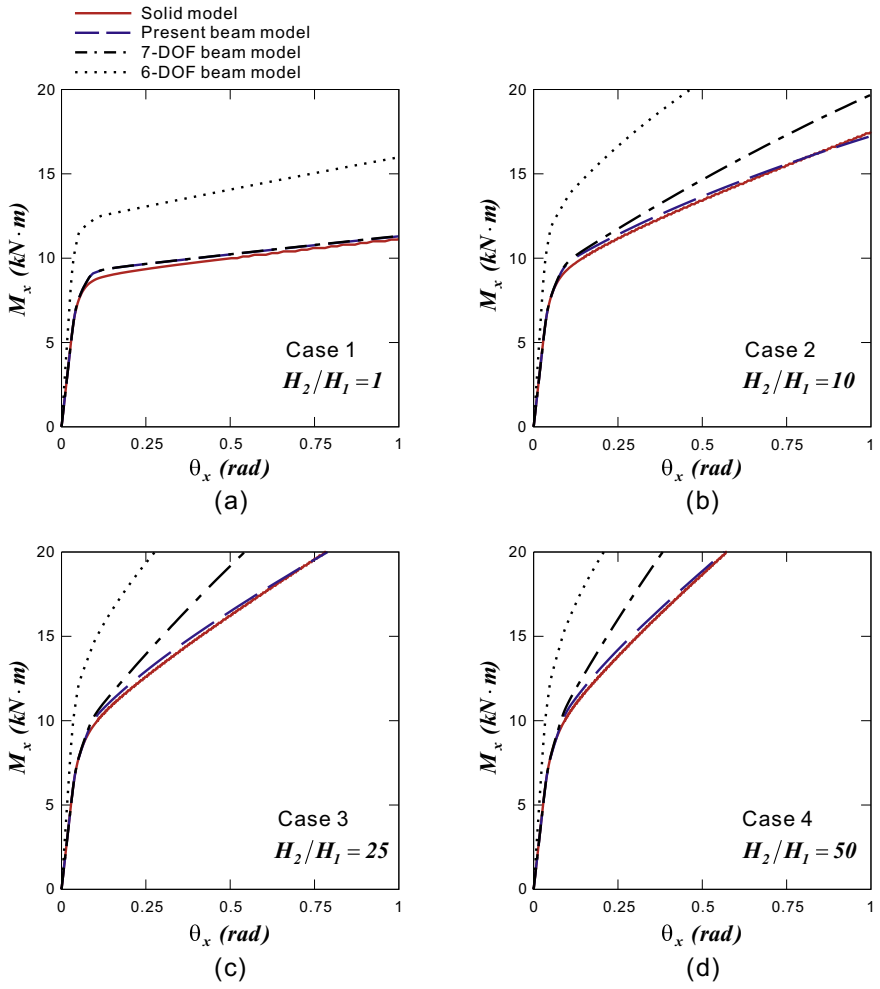

Fig. 5. Moment-angle curves in the double layered beam problem.

and $\partial\tau^{(m)}/\partial\gamma_e^{(m)} = G_e^{(m)}$, Eq. (19) can be written as

$$G_{ep}^{(m)} = \frac{H^{(m)}G_e^{(m)}}{H^{(m)} + 3G_e^{(m)}}. \tag{21}$$

Finally, we can compute the asymptotic plastic warping function $\mathbf{F}_p = [f_p^1 \quad f_p^2 \quad \cdots \quad f_p^I]^T$ by solving Eq. (12) with the substitution of $E_{ep}^{(m)}$ and $G_{ep}^{(m)}$ in Eqs. (18) and (21) for $E_e^{(m)}$ and $G_e^{(m)}$ in Eq. (13).

4. Beam finite element formulation

To obtain the nonlinear elastoplastic response of composite beams, we use the total Lagrangian formulation for the beam element defined in the local Cartesian coordinate system [29–31] given by

$$\int_{0V} \bar{C}_{ijkl}^{ep}{}_0\bar{e}_{ij}\delta_0\bar{e}_{kl}d^0V + \int_{0V} {}_0^t\bar{S}_{ij}\delta_0\bar{\eta}_{ij}d^0V + \int_{0V} {}_0^t\bar{S}_{ij}\delta_0\bar{\kappa}_{ij}d^0V = {}^{t+\Delta t}\Re - \int_{0V} {}_0^t\bar{S}_{ij}\delta_0\bar{e}_{ij}d^0V, \tag{22}$$

in which ${}_0\bar{e}_{ij}$ is the linear strain term from the first order part of the incremental Green-Lagrange strain, ${}_0\bar{\eta}_{ij}$ is the nonlinear strain term from the second order part of the incremental Green-Lagrange strain, ${}_0\bar{\kappa}_{ij}$ is the nonlinear strain term from the second order rotational displacements, ${}^0V$ is the volume of a beam element at time 0, ${}^{t+\Delta t}\Re$ is the external virtual work due to the applied surface tractions and body forces, and $\bar{C}_{ijkl}^{ep}$ and ${}_0^t\bar{S}_{ij}$ denote the elastoplastic stress-strain law and the second Piola-Kirchhoff stress, respectively.

The covariant Green-Lagrange strain components ${}_0^t\varepsilon_{ij}^{(m)}$ for sub-beam m are defined as

$${}_0^t\boldsymbol{\varepsilon}^{(m)} = \begin{bmatrix} {}_0^t\varepsilon_{11}^{(m)} & 2{}_0^t\varepsilon_{12}^{(m)} & 2{}_0^t\varepsilon_{13}^{(m)} \end{bmatrix}^T \quad \text{with}$$
$${}_0^t\varepsilon_{ij}^{(m)} = \frac{1}{2}({}^t\mathbf{g}_i^{(m)} \cdot {}^t\mathbf{g}_j^{(m)} - {}^0\mathbf{g}_i^{(m)} \cdot {}^0\mathbf{g}_j^{(m)}) \tag{23a}$$

in which

$${}^t\mathbf{g}_i^{(m)} = \frac{\partial {}^t\mathbf{x}^{(m)}}{\partial r_i} \text{ with } r_1 = \varsigma,\ r_2 = \xi,\ \text{and } r_3 = \eta. \tag{23b}$$

Note that the other strain components are assumed by zero through the kinematic assumption of Timoshenko beam theory [29–31]. In order to avoid shear and membrane locking phenomena, we use the assumed covariant Green-Lagrange strain components instead,

$${}_0^t\boldsymbol{\varepsilon}^{AS(m)} = \begin{bmatrix} {}_0^t\varepsilon_{11}^{AS(m)} & 2{}_0^t\varepsilon_{12}^{AS(m)} & 2{}_0^t\varepsilon_{13}^{AS(m)} \end{bmatrix}^T \tag{24}$$

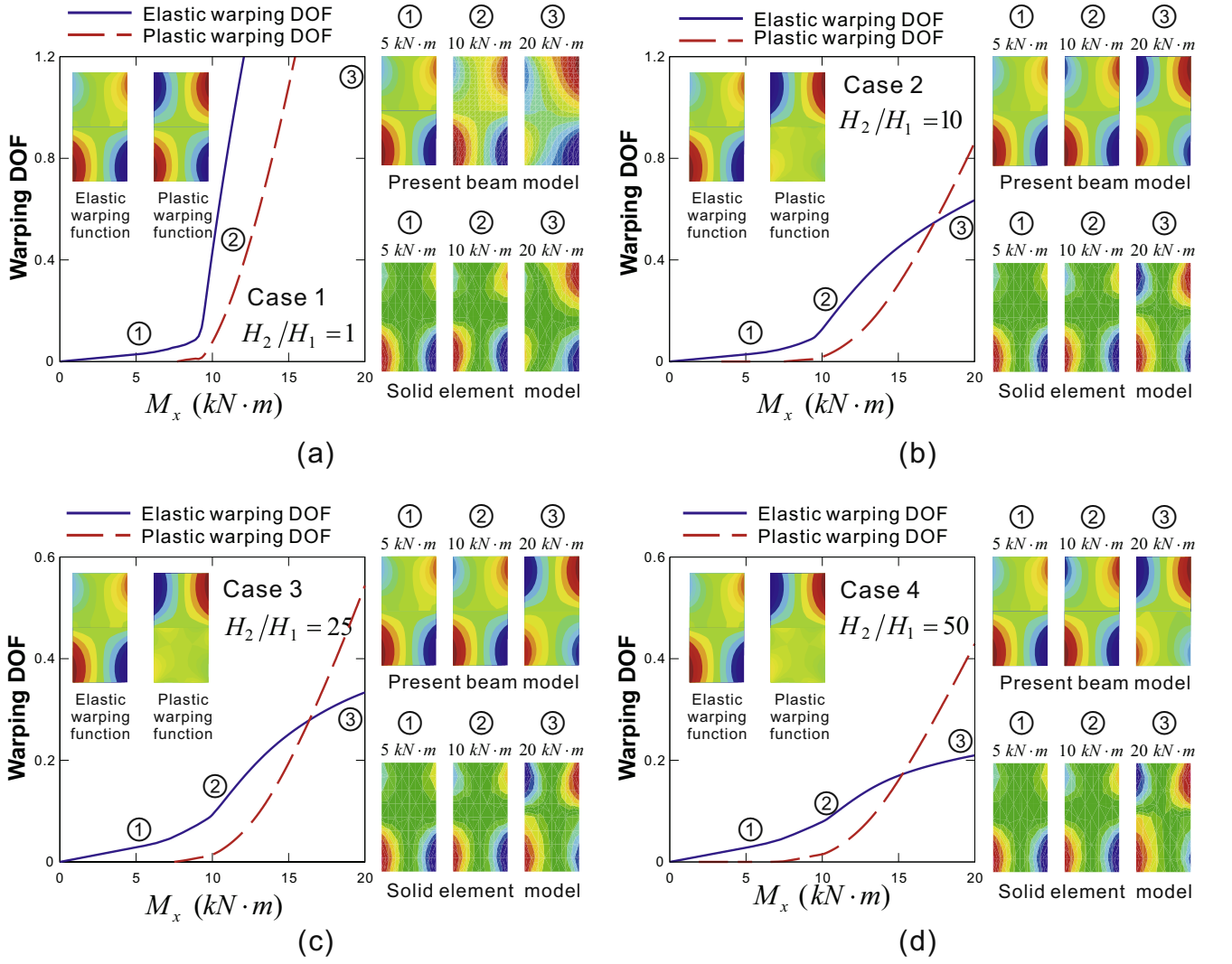

Fig. 6. Evolution of the elastic and plastic warping DOFs (left) and the axial displacements on a cross-section (right) at $x = 1m$ in the double layered beam problem.

by employing the well-established MITC (Mixed Interpolation of Tensorial Components) scheme [31–33]. The strain components are then transformed into the local Cartesian coordinate system using

$$
\begin{aligned}
&{}^{t}_{0}\bar{\boldsymbol{\varepsilon}}^{(m)} = \begin{bmatrix} {}^{t}_{0}\bar{\varepsilon}^{(m)}_{11} & 2{}^{t}_{0}\bar{\varepsilon}^{(m)}_{12} & 2{}^{t}_{0}\bar{\varepsilon}^{(m)}_{13} \end{bmatrix}^{T} \quad \text{with} \\
&{}^{t}_{0}\bar{\varepsilon}^{(m)}_{ij}({}^{0}\mathbf{t}_i \otimes {}^{0}\mathbf{t}_j) = {}^{t}_{0}\varepsilon^{AS(m)}_{kl}({}^{0}\mathbf{g}^{k(m)} \otimes {}^{0}\mathbf{g}^{l(m)}),
\end{aligned}
\tag{25}
$$

where the base vectors of the local Cartesian coordinate system are defined as

$$
{}^{0}\mathbf{t}_1 = h_k(\varsigma){}^{0}\mathbf{V}^{k}_{\bar{x}}, \quad {}^{0}\mathbf{t}_2 = h_k(\varsigma){}^{0}\mathbf{V}^{k}_{\bar{y}} \quad \text{and} \quad {}^{0}\mathbf{t}_3 = h_k(\varsigma){}^{0}\mathbf{V}^{k}_{\bar{z}}. \tag{26}
$$

and ${}^{0}\mathbf{g}^{i(m)}$ represent the contravariant base vectors satisfying

$$
{}^{0}\mathbf{g}^{i(m)} \cdot {}^{0}\mathbf{g}^{(m)}_{j} = \delta^{i}_{j}, \tag{27}
$$

in which δ^{i}_{j} denotes the Kronecker delta ($\delta^{i}_{j} = 1$ if $i = j$, and 0 otherwise). They are split into elastic components and plastic components,

$$
{}^{t}_{0}\bar{\boldsymbol{\varepsilon}}^{(m)} = {}^{t}_{0}\bar{\boldsymbol{\varepsilon}}^{(m)}_{e} + {}^{t}_{0}\bar{\boldsymbol{\varepsilon}}^{(m)}_{p}. \tag{28}
$$

so that the second Piola-Kirchhoff stresses are calculated using

$$
{}^{t}_{0}\bar{S}^{(m)} = \bar{\mathbf{C}}^{(m)}_{e}{}^{t}_{0}\bar{\boldsymbol{\varepsilon}}^{(m)}_{e} \tag{29a}
$$

$$
\text{with } {}^{t}_{0}\bar{S}^{(m)} = \begin{bmatrix} {}^{t}_{0}\bar{S}^{(m)}_{11} & {}^{t}_{0}\bar{S}^{(m)}_{12} & {}^{t}_{0}\bar{S}^{(m)}_{13} \end{bmatrix}^{T} \text{ and } \bar{\mathbf{C}}^{(m)}_{e} = \begin{bmatrix} E^{(m)}_{e} & 0 & 0 \\ 0 & G^{(m)}_{e} & 0 \\ 0 & 0 & G^{(m)}_{e} \end{bmatrix}. \tag{29b}
$$

Conventional implicit return mapping algorithm is used for their determination [31,34–36].The incremental DOFs of a q-node beam element are

$$
{}_{0}\mathbf{U} = \begin{bmatrix} {}_{0}\mathbf{U}^{T}_{1} & {}_{0}\mathbf{U}^{T}_{2} & \cdots & {}_{0}\mathbf{U}^{T}_{q} \end{bmatrix}^{T} \tag{30a}
$$

$$
\text{with } {}_{0}\mathbf{U}_k = \begin{bmatrix} {}_{0}u_k & {}_{0}v_k & {}_{0}w_k \,|\, & {}_{0}\theta^{k}_{x} & {}_{0}\theta^{k}_{y} & {}_{0}\theta^{k}_{z} | & {}_{0}\alpha^{e}_{k} & {}_{0}\alpha^{p}_{k} \end{bmatrix}^{T} \tag{30b}
$$

in which ${}_{0}\mathbf{U}_k$ is a vector of the nodal DOFs at beam node k consisting of eight (three translations, three rotations, and two warping) DOFs. To update properly the director vectors considering a large rotation, the finite rotation matrix is employed here

$$
\mathbf{R}({}_{0}\boldsymbol{\theta}^{k}) = \mathbf{I} + \frac{\sin {}_{0}\theta^{k}}{{}_{0}\theta^{k}}\hat{\mathbf{R}}({}_{0}\boldsymbol{\theta}^{k}) + \frac{1-\cos {}_{0}\theta^{k}}{({}_{0}\theta^{k})^{2}}\hat{\mathbf{R}}({}_{0}\boldsymbol{\theta}^{k})^{2} \tag{31a}
$$

$$
\begin{aligned}
&\text{with } {}_{0}\boldsymbol{\theta}^{k} = \begin{bmatrix} {}_{0}\theta^{k}_{x} & {}_{0}\theta^{k}_{y} & {}_{0}\theta^{k}_{z} \end{bmatrix}^{T}, \; {}_{0}\theta^{k} = \|{}_{0}\boldsymbol{\theta}^{k}\|, \\
&\hat{\mathbf{R}}({}_{0}\boldsymbol{\theta}^{k}) = \begin{bmatrix} 0 & -{}_{0}\theta^{k}_{z} & {}_{0}\theta^{k}_{y} \\ {}_{0}\theta^{k}_{z} & 0 & -{}_{0}\theta^{k}_{x} \\ -{}_{0}\theta^{k}_{y} & {}_{0}\theta^{k}_{x} & 0 \end{bmatrix}.
\end{aligned}
\tag{31b}
$$

Then, the incremental strains in Eq. (22) can be written as

$$
{}_{0}\bar{e}^{(m)}_{ij} = \bar{\mathbf{B}}^{(m)}_{ij}{}_{0}\mathbf{U}, \tag{32a}
$$

$$
{}_{0}\bar{\eta}^{(m)}_{ij} = \frac{1}{2}{}_{0}\mathbf{U}^{T}{}_{1}\bar{\mathbf{N}}^{(m)}_{ij}{}_{0}\mathbf{U}, \tag{32b}
$$

$$
{}_{0}\bar{\kappa}^{(m)}_{ij} = \frac{1}{2}{}_{0}\mathbf{U}^{T}{}_{2}\bar{\mathbf{N}}^{(m)}_{ij}{}_{0}\mathbf{U} \tag{32c}
$$

where $\bar{\mathbf{B}}^{(m)}_{ij}$, ${}_{1}\bar{\mathbf{N}}^{(m)}_{ij}$ and ${}_{2}\bar{\mathbf{N}}^{(m)}_{ij}$ are matrices that relate the incremental strains to the incremental DOFs vector. The detailed form of these matrices is available in Ref. [31]. Substituting Eq. (32) into Eq. (22) leads to the following discretized equations

$$
\begin{aligned}
&\delta_{0}\mathbf{U}^{T}\left[\sum_{m=1}^{n}\int_{{}_{0}V^{(m)}}\bar{\mathbf{B}}^{(m)T}_{ij}\bar{C}^{ep}_{ijkl}\bar{\mathbf{B}}^{(m)}_{kl}d^{0}V^{(m)} + \sum_{m=1}^{n}\int_{{}_{0}V^{(m)}}{}_{1}\bar{\mathbf{N}}^{(m)}_{ij}{}^{t}_{0}\bar{S}_{ij}d^{0}V^{(m)}\right. \\
&\quad \left. + \sum_{m=1}^{n}\int_{{}_{0}V^{(m)}}{}_{2}\bar{\mathbf{N}}^{(m)}_{ij}{}^{t}_{0}\bar{S}_{ij}d^{0}V^{(m)}\right]{}_{0}\mathbf{U} \\
&\quad = \delta_{0}\mathbf{U}^{T}{}^{t+\Delta t}\mathbf{R} - \delta_{0}\mathbf{U}^{T}\left[\sum_{m=1}^{n}\int_{{}_{0}V^{(m)}}\bar{\mathbf{B}}^{(m)T}_{ij}{}^{t}_{0}\bar{S}_{ij}d^{0}V^{(m)}\right],
\end{aligned}
\tag{33}
$$

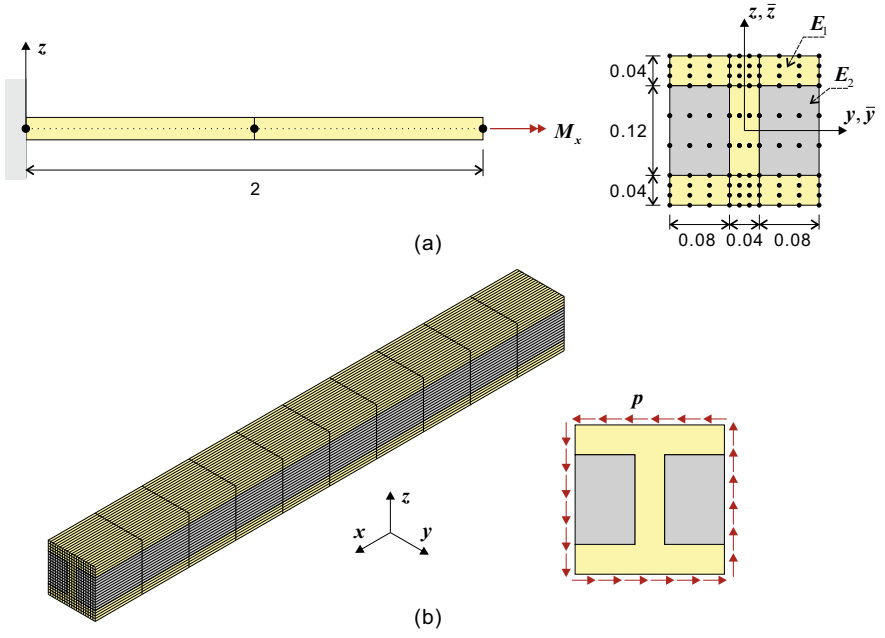

Fig. 7. Reinforced wide-flange beam problem (unit: m): (a) beam model (two beam elements along the beam axis, nine cubic cross-sectional elements, 24 DOFs in total) and (b) solid model (4000 solid elements, 14,553 DOFs in total).

where ${}^0V^{(m)}$ is the initial volume of the sub-beam m and ${}^0V = \sum_{m=1}^{n} {}^0V^{(m)}$. Finally, the incremental equilibrium equations to be solved can be written as

$$ {}^t\mathbf{K}_0\mathbf{U} = {}^{t+\Delta t}\mathbf{R} - {}^t_0\mathbf{F} \quad \text{with} \quad {}^t\mathbf{K} = {}^t\mathbf{K}_L + {}^t_1\mathbf{K}_{NL} + {}^t_2\mathbf{K}_{NL}, \tag{34} $$

where

$$ {}^t\mathbf{K}_L = \sum_{m=1}^{n} \int_{{}^0V^{(m)}} \bar{\mathbf{B}}_{ij}^{(m)^T} \bar{C}^{ep}_{ijkl} \bar{\mathbf{B}}_{kl}^{(m)} dV^{(m)}, \tag{35a} $$

$$ {}^t_1\mathbf{K}_{NL} = \sum_{m=1}^{n} \int_{{}^0V^{(m)}} {}_1\bar{\mathbf{N}}_{ij}^{(m)} {}^t_0\bar{S}_{ij} dV^{(m)}, \tag{35b} $$

$$ {}^t_2\mathbf{K}_{NL} = \sum_{m=1}^{n} \int_{{}^0V^{(m)}} {}_2\bar{\mathbf{N}}_{ij}^{(m)} {}^t_0\bar{S}_{ij} dV^{(m)}, \tag{35c} $$

$$ {}^t_0\mathbf{F} = \sum_{m=1}^{n} \int_{{}^0V^{(m)}} \bar{\mathbf{B}}_{ij}^{(m)^T} {}^t_0\bar{S}_{ij} dV^{(m)}. \tag{35d} $$

5. Numerical examples

In this section, we demonstrate the performance of the proposed warping model by solving several numerical examples. The first example investigates the performance of the proposed warping formulation for various hardening moduli of composite materi-

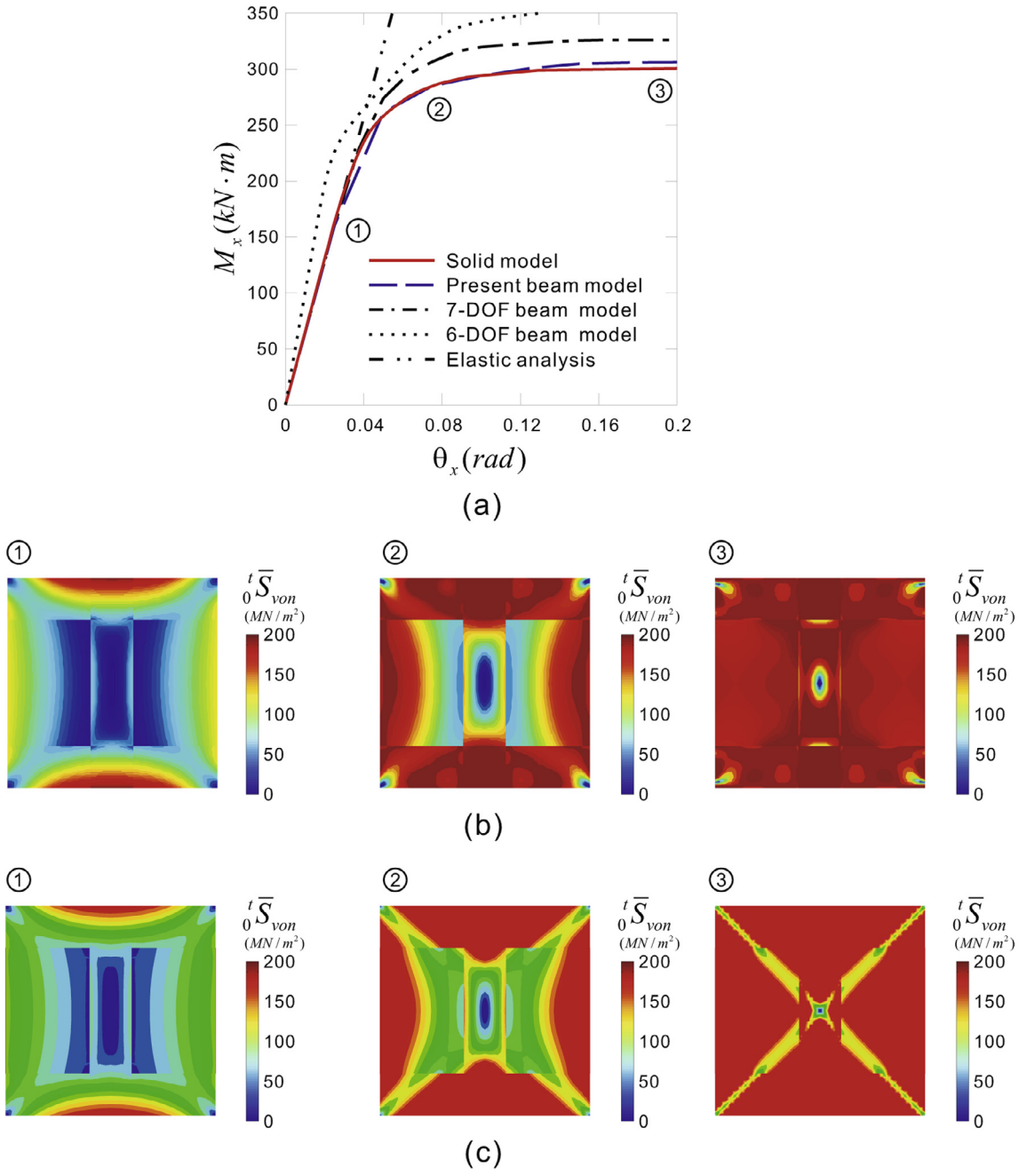

Fig. 8. Results of the reinforced wide-flange beam problem: (a) moment-angle curves and the distribution of von Mises stresses at $x = 0.5\,m$ obtained using (b) the present beam model and (c) the solid model.

als. The elastoplastic response of a reinforced wide-flange beam is then investigated in detail followed by our test of the beam in highly nonlinear post-buckling problems. Finally, the results for a beam under cyclic loadings are presented.

The standard full Newton-Raphson iterative scheme is employed to solve Eq. (34) for these nonlinear problems. Two and sixteen gauss quadrature points are used for numerical integration along the beam axis and within the cross-section, respectively. Here, we use a linear isotropic hardening model for illustration purposes within the von Mises plasticity so that the asymptotic plastic tangent moduli in Eqs. (18) and (21) become constant. Results obtained using the present beam model are compared with those calculated using a 6-DOF beam model, a 7-DOF beam model and a reference 3D solid model where the 6-DOF beam model represents a conventional Timoshenko beam without the warping effect and the 7-DOF beam model is different from the present beam model in that it considers the elastic warping function only. The reference solutions with a 3D solid model are obtained by using commercial finite element analysis software, ADINA [37].

5.1. Double layered beam problem

We consider a straight cantilever beam with double layered rectangular cross-section whose length L is $1\,m$ as shown in Fig. 4(a). It is modeled using four 2-node beam elements whose cross-sections are discretized using two cubic cross-sectional elements. The clamped boundary condition $u = v = w = \theta_x = \theta_y = \theta_z = \alpha_e = \alpha_p = 0$ is applied at one end while a torsional moment M_x is applied at the other end. Each layer has the following material properties:

- Material 1 (yellow colored in Fig. 4): Young's modulus $E_1 = 200$ GPa, shear modulus $G_1 = 100$ GPa, the initial yield stress $Y_1 = 200$ MPa, and the linear hardening modulus $H_1 = 2$ GPa.
- Material 2 (gray colored in Fig. 4): Young's modulus $E_2 = 70$ GPa, Shear modulus $G_2 = 35$ GPa, the initial yield stress $Y_2 = 100$ MPa, and the linear hardening moduli $H_2 = 2,\ 20,\ 50,\ 100$ GPa.

The reference solutions are obtained using a 3D solid model consisting of three hundred twenty 27-node solid elements where the torsional moment is applied by using rigid links as shown in Fig.4(b). Fig. 5 shows the torsional moment-angle curves obtained using the present, 7-DOF, and 6-DOF beam models as well as the reference solid element model for various ratios of hardening moduli. Results obtained using the present beam model are almost identical to the reference solutions for any combination of hardening moduli. The 7-DOF beam model results begin to deviate significantly from the reference ones after initial yield because it has the elastic warping DOF only. Nevertheless, when the hardening modulus of two materials is the same, it is observed that the solutions obtained using the present and 7-DOF beam models are almost identical as shown in Fig. 5(a). This is because the difference between the elastic and plastic warping functions are relatively small and the elastic warping has a primary effect as shown in Fig. 6(a). In all the other cases, the plastic warping functions are quite different from the elastic ones and the plastic warping becomes dominant after a certain magnitude of torsion is applied. The axial displacements on a cross-section obtained using the present beam model are well matched with the reference axial displacements demonstrating the usefulness and effectiveness of the proposed warping model (Fig. 6). It is not surprising that the 6-DOF beam model provides unreliable solutions as it does not account for the warping effect at all.

5.2. Reinforced wide-flange beam problem

We consider a straight cantilever beam with reinforced wide-flange cross-section whose length L is $2\,m$ as shown in Fig. 7(a). It is modeled using two 2-node beam elements whose cross-sections are discretized using nine cubic cross-sectional elements. The clamped boundary condition $u = v = w = \theta_x = \theta_y = \theta_z = \alpha_e = \alpha_p = 0$ is applied at one end while a torsional moment M_x is applied at the other end. The beam consists of steel (Material 1) and high strength concrete (Material 2) whose material properties are:

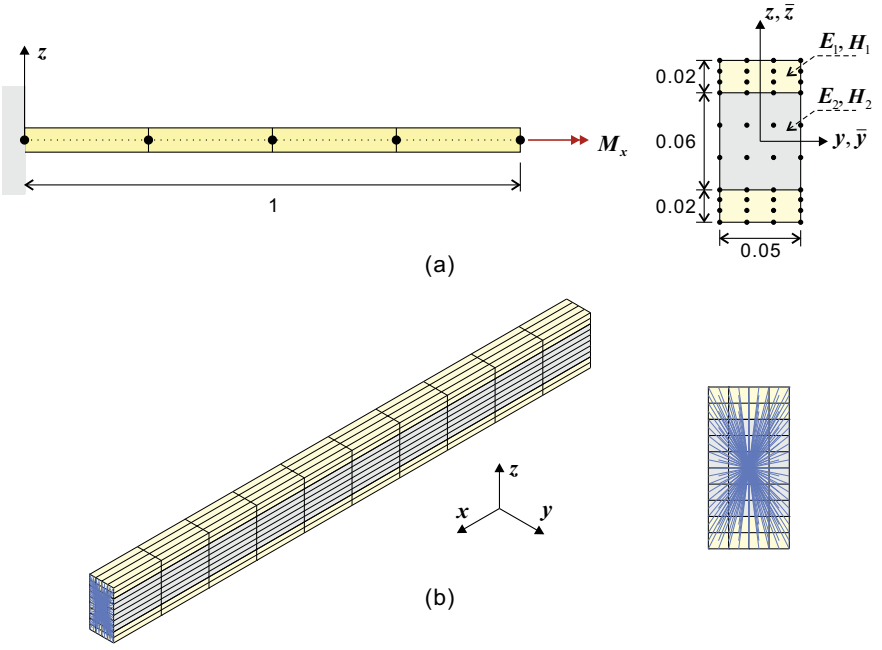

Fig. 9. Sandwich beam under cyclic loading problem (unit: m): (a) beam model (four beam elements along the beam axis, three cubic cross-sectional elements, 40 DOFs in total) and (b) solid model (400 solid elements, 11,907 DOFs in total).

- Material 1 (yellow colored in Fig. 7): Young's modulus $E_1 = 200$ GPa, shear modulus $G_1 = 100$ GPa, the initial yield stress $Y_1 = 200$ MPa, and the elastic perfectly plastic materials (zero hardening modulus).
- Material 2 (gray colored in Fig. 7): Young's modulus $E_2 = 70$ GPa, shear modulus $G_2 = 35$ GPa, the initial yield stress $Y_2 = 200$ MPa, and the elastic perfectly plastic materials (zero hardening modulus).

The reference solutions are obtained using a 3D solid model consisting of four thousand 8-node solid elements where the torsional moment is applied as a distributed line load of $p = 12.5M_x$ along the outer edges of the cross-section at the free end as shown in Fig. 7(b).

Results clearly illustrate that the present beam model can predict the limit torsional moment accurately close to the reference solution as shown in Fig. 8(a). Notably, the 7-DOF beam model predicts a significantly (about 10%) higher value for this moment, which would be dangerous to be used in a structural design where the limit load is of importance. Comparison of the von Mises stress on a cross-section reveals that the key features of the propagation of plastic regions can be reasonably captured using the proposed, simple treatment for warping.

5.3. Sandwich beam under cyclic load problem

We consider a straight cantilever beam with sandwich cross-section whose length L is 1 m as shown in Fig. 9(a). It is modeled using four 2-node beam elements whose cross-sections are discretized using three cubic cross-sectional elements. The clamped boundary condition $u = v = w = \theta_x = \theta_y = \theta_z = \alpha_e = \alpha_p = 0$ is applied at one end while a cyclic torsional moment M_x is applied at the other end. The material properties of comprising materials are:

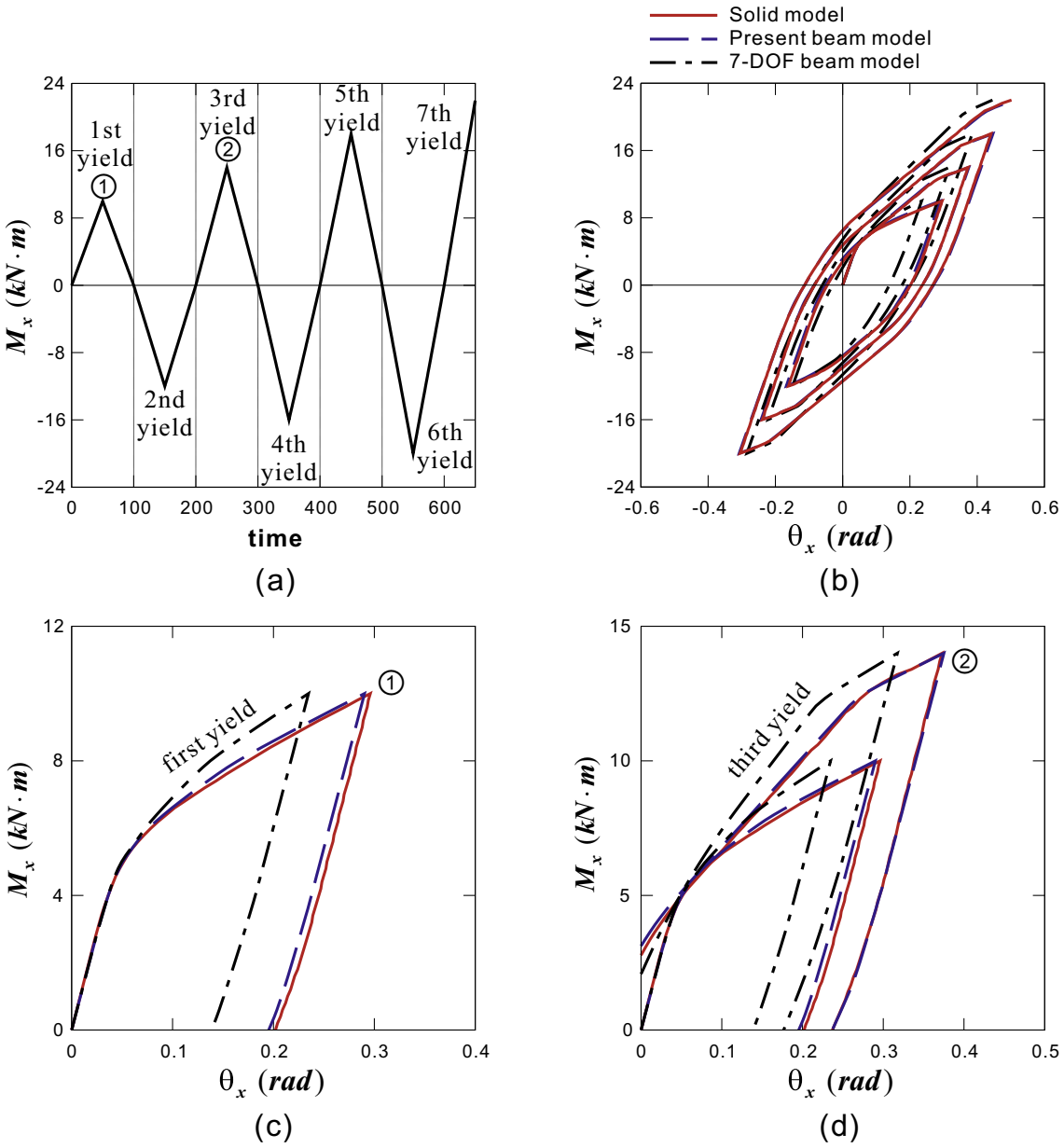

Fig. 10. Results of the sandwich beam under cyclic loading problem: (a) time history of the applied torsional moment and moment-angle curves (b) in the entire time history, (c) near the first yield, and (d) near the third yield.

- Material 1 (yellow colored in Fig. 9): Young's modulus $E_1 = 200$ GPa, shear modulus $G_1 = 100$ GPa, the initial yield stress $Y_1 = 100$ MPa, and the linear hardening modulus $H_1 = 2$ GPa.
- Material 2 (gray colored in Fig. 9): Young's modulus $E_2 = 50$ GPa, shear modulus $G_2 = 25$ GPa, the initial yield stress $Y_2 = 100$ MPa, and the linear hardening modulus $H_2 = 20$ GPa.

The reference solutions are obtained using a 3D solid model consisting of four hundred 27-node solid elements where the torsional moment is applied by using rigid links as shown in Fig. 9(b). Fig. 10(a) shows the history of the applied torsional moment M_x whose maximum value is increased whenever the load is reversed so that yield occurs seven times in total. The cyclic moment-angle curve obtained using the present beam model shows an excellent performance of the proposed method in describing the nonlinear torsional behavior of composite beams even under cyclic loading-unloading conditions. The use of the present beam model would be much more efficient computationally when solving this kind of complex problems because we only need to update two warping DOFs only during analysis without evaluating the warping functions again. As expected, the use of a single, elastic warping DOF fails to reproduce the reference solution.

5.4. Lateral post-buckling problem

Finally we consider a straight cantilever beam with T-shaped cross-section whose length L is 2 m as shown in Fig. 11(a). It is modeled using eight 2-node beam elements whose cross-sections are discretized using four cubic cross-sectional elements. The clamped boundary condition $u = v = w = \theta_x = \theta_y = \theta_z = \alpha_e = \alpha_p = 0$ is applied at one end while two loading cases where the

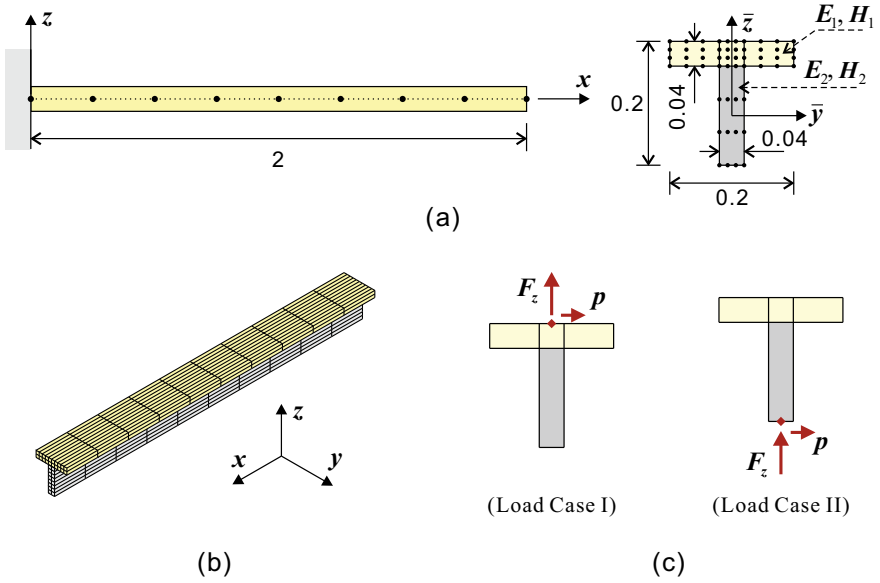

Fig. 11. Lateral post-buckling problem (unit: m): (a) beam model (eight beam elements along the beam axis, seven cubic cross-sectional elements, 72 DOFs in total), (b) solid model (360 solid elements, 11,655 DOFs in total) and (c) two loading conditions.

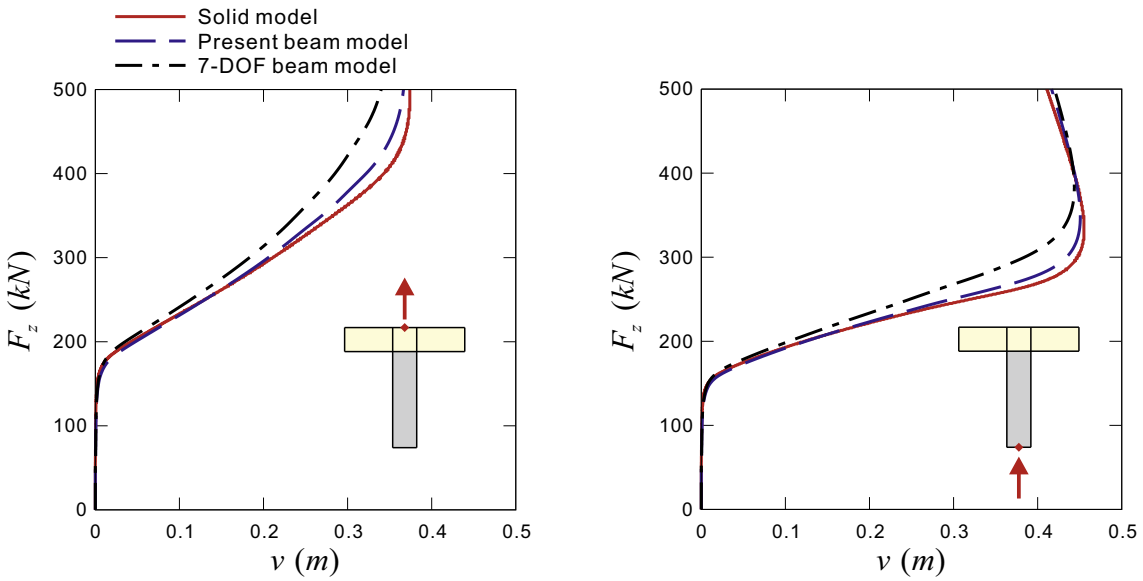

Fig. 12. Load-displacement curves for two loading conditions in the lateral post-buckling problem.

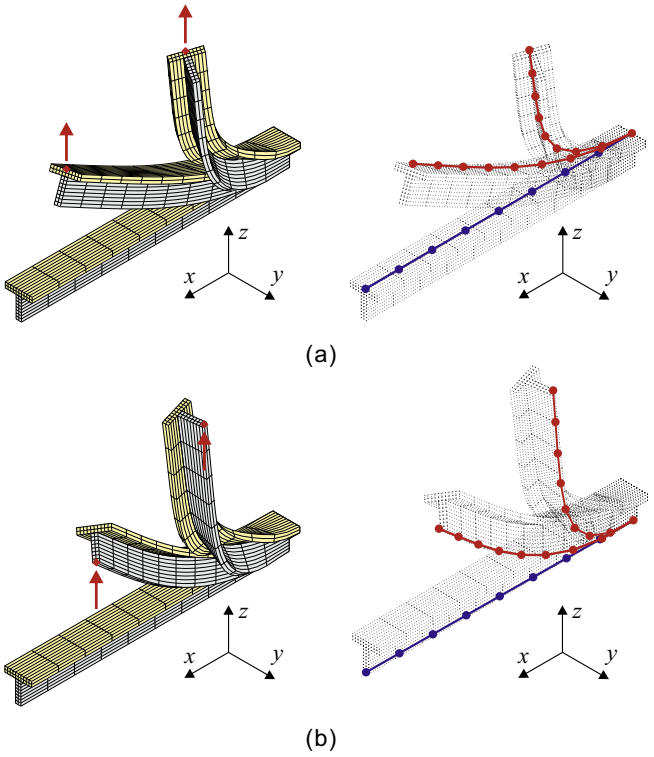

Fig. 13. Initial and deformed configurations obtained using the solid model and the present beam model when $F_z = 250$ and 500 kN in the lateral post-buckling problem: (a) Load Case I and (b) Load Case II.

same point force is applied either on the top or on the bottom are considered as shown in Fig. 11(b). A small lateral perturbation load ($p = 10N$) is applied together to model an imperfection. The material properties of comprising materials are:

- Material 1 (yellow colored in Fig. 11): Young's modulus $E_1 = 200$ GPa, shear modulus $G_1 = 100$ GPa, the initial yield stress $Y_1 = 100$ MPa, and the linear hardening modulus $H_1 = 2$ GPa.
- Material 2 (gray colored in Fig. 11): Young's modulus $E_2 = 70$ GPa, shear modulus $G_2 = 35$ GPa, the initial yield stress $Y_2 = 50$ MPa, and the linear hardening modulus $H_2 = 50$ GPa.

The reference solutions are obtained using a 3D solid model consisting of three hundred sixty 27-node solid elements.

Figs. 12 and 13 present the lateral post-buckling responses and the corresponding deformed configurations, respectively, for two different loading cases. The beam undergoes pure bending until the applied load reaches to a critical buckling load. Then, it exhibits the lateral displacements showing coupled twist-bend deformations. Two different post-buckling responses of the beam dependent on the load position are accurately reproduced using the present beam model. Using the 7-DOF beam model deteriorates the response in the region of coupled twist-bend deformation. This result confirms that the present beam model can be used effectively for problems where twist-bend deformations are highly coupled.

6. Conclusions

We present in this paper an efficient method to represent the intricate warping effect for elastoplastic torsional analysis of composite beams. The proposed method models the elastoplastic warping function, which evolves with the plastic deformation, as a linear combination of two asymptotic warping functions. These functions are calculated first before performing nonlinear analysis by solving the extended St. Venant equations under two conditions: purely elastic and fully plastic conditions. Corresponding warping DOFs are only updated during analysis without calculating the warping function again, which makes the method computationally efficient. An excellent performance of the proposed method is demonstrated in several numerical examples.

Acknowledgments

This work was supported by the Convergence Research Program for Sports Scientification through the National Research Foundation of Korea (NRF) funded by the Ministry of Science, ICT & Future Planning (2014M3C1B1033983) and also by EDucation-research Integration through Simulation On the Net (EDISON) Program (2014M3C1A6038842).

References

[1] Jones RM. Mechanics of composite materials. McGrawHill; 1975.
[2] Reddy JN. Mechanics of laminated composite plates: theory and analysis. New York: CRC Press; 1997.
[3] Hodges DH. Nonlinear composite beam theory. New York: AIAA; 2006.
[4] Kara IF, Ashour AF, Köroğlu MA. Flexural performance of reinforced concrete beams strengthened with prestressed near-surface-mounted FRP reinforcements. Compos Part B Eng 2016;91:371–83.
[5] Jung JD, Becker W. Semi-analytical modeling of composite beams using the scaled boundary finite element method. Compos Struct 2016;137:121–9.
[6] Peterson KL, Underhill J, Carlson B, Heyliger PR. The mechanics of plastic-aluminum composite I-beams. Compos Struct 2016;136:241–50.
[7] Sheikh AH, Thomsen OT. An efficient beam element for the analysis of laminated composite beams. Compos Sci Technol 2008;68:2273–81.
[8] Lee J. Flexural analysis of thin-walled composite beams using shear-deformable beam theory. Compos Struct 2005;70:212–22.
[9] Vo TP, Lee J. Free vibration of thin-walled composite box beams. Compos Struct 2007;84:11–20.
[10] Chakravarty UK. On the modeling of composite beam cross-sections. Compos Part B Eng 2011;42:982–91.
[11] Pisano AA, Fuschi P. A numerical approach for limit analysis of orthotropic composite laminates. Int J Numer Methods Eng 2007;70:71–93.
[12] Kiral BG, Kiral Z, Ozturk H. Stability analysis of delaminated composite beams. Compos Part B Eng 2015;79:406–18.
[13] Wackerfuß J, Gruttman F. A nonlinear Hu-Washizu variational formulation and related finite-element implementation for spatial beams with arbitrary moderate thick cross-sections. Comput Meth Appl Mech Eng 2011;200:1671–90.
[14] Lee PS, McClure G. A general three-dimensional L-section beam finite element for elastoplastic large deformation analysis. Comput Struct 2006;84:215–29.
[15] Ayoub A, Fillppou FC. Mixed formulation of nonlinear steel-concrete composite beam element. J Struct Eng 2000;126:371–81.
[16] Yoon K, Lee YG, Lee PS. A continuum mechanics based beam finite element with warping displacements and its modeling capabilities. Strut Eng Mech 2012;43:411–37.
[17] Yoon K, Lee PS, Kim DN. Geometrically nonlinear finite element analysis of functionally graded 3D beams considering warping effects. Compos Struct 2015;132:1231–47.
[18] Mancusi G, Feo L. Non-linear pre-buckling behavior of shear deformable thin-walled composite beams with open cross-section. Compos Part B Eng 2013;47:379–90.
[19] Wagner W, Gruttmann F. A displacement method for the analysis of flexural shear stresses in thin-walled isotropic composite beams. Comput Struct 2002;80:1843–51.
[20] Genoese A, Genoese A, Bilotta A, Garcea G. A composite beam model including variable warping effects derived from a generalized Saint Venant solution. Compos Struct 2013;110:140–51.
[21] Fatmi REI, Ghazouani N. Higher order composite beam theory built on Saint-Venant's solution. Part-I: theoretical developments. Compos Struct 2011;93:557–66.
[22] Qureshi MAM, Rao HG. Torsional response of closed FRP composite sections. Compos Part B Eng 2014;61:254–66.
[23] Barretta R, Luciano R, Willis JR. On torsion of random composite beams. Compos Struct 2015;132:915–22.
[24] Sapountzakis EJ, Mokos VG. Warping shear stresses in nonuniform torsion of composite bars by BEM. Comput Meth Appl Mech Eng 2003;192:4337–53.
[25] Sapountzakis EJ, Tsipiras VJ. Nonlinear inelastic uniform torsion of composite bars by BEM. Comput Struct 2009;87:151–66.
[26] Benscoter SU. A theory of torsion bending for multicell beams. J Appl Mech 1954;21:25–34.

[27] Shakourzadeth H, Guo YQ, Batoz JL. A torsion bending element for thin-walled beams with open and closed cross sections. Comput Struct 1995;55:1045–54.
[28] Yoon K, Lee PS. Modeling the warping displacements for discontinuously varying arbitrary cross-section beams. Comput Struct 2014;131:56–69.
[29] Bathe KJ. Finite element precedures, 2nd ed. Watertown, (MA): KJ Bathe; 2014.
[30] Dvorkin EN, Onate E, Oliver J. On a non-linear formulation for curved Timoshenko beam elements considering large displacement/rotation increments. Int J Numer Meth Eng 1988;26:1597–613.
[31] Yoon K, Lee PS. Nonlinear performance of continuum mechanics based beam elements focusing on large twisting behaviors. Comput Meth Appl Mech Eng 2014;281:106–30.
[32] Kim DN, Bathe KJ. A 4-node 3D-shell element to model shell surface tractions and incompressible behavior. Comput Struct 2008;86:2027–41.
[33] Kim DN, Bathe KJ. A triangular six-node shell element. Comput Struct 2009;87:1451–60.
[34] Neto EAS, Peric D, Owen DRJ. Computational method for plasticity: theory and applications. Wiley & Sons; 2008.
[35] Kim DN, Montans FJ, Bathe KJ. Insight into a model for large strain anisotropic elasto-plasticity. Comput Mech 2009;44:651–68.
[36] Ortiz M, Simo JC. An analysis of a new class of integration algorithms for elastoplastic constitutive relations. Int J Numer Meth Eng 1986;23:353–66.
[37] ADINA R&D, ADINA theory and modeling guide, Watertown, MA: ADINA R&D; 2013.